REVIEWS

Journal of Semiconductors
(2019) 40, 081502
doi: 10.1088/1674-4926/40/8/081502
JOS

Magnetization dynamics and related phenomena in semiconductors with ferromagnetism

Lin Chen[1, †], Jianhua Zhao[2], Dieter Weiss[1], Christian H. Back[3, 1], Fumihiro Matsukura[4], and Hideo Ohno[4, 5]

[1]Institute of Experimental and Applied Physics, University of Regensburg, 93049 Regensburg, Germany

[2]State Key Laboratory of Superlattices and Microstructures, Institute of Semiconductors, Chinese Academy of Sciences, Beijing 100083, China

[3]Department of Physics, Technical University of Munich, Garching b. Munich, Germany

[4]Center for Innovative Integrated Electronic Systems, Tohoku University, Sendai 980-0845, Japan

[5]Laboratory for Nanoelectronics and Spintronics, Research Institute of Electrical Communication, Tohoku University, Sendai 980-8577, Japan

Abstract: We review ferromagnetic resonance (FMR) and related phenomena in the ferromagnetic semiconductor (Ga,Mn)As and single crystalline Fe/GaAs (001) hybrid structures. In both systems, spin-orbit interaction is the key ingredient for various intriguing phenomena.

Key words: (Ga,Mn)As; Fe/GaAs; ferromagnetic resonance; Gilbert damping; electric-field effect on magnetism; spin-orbit fields

Citation: L Chen, J H Zhao, D Weiss, C H Back, F Matsukura, and H Ohno, Magnetization dynamics and related phenomena in semiconductors with ferromagnetism[J]. *J. Semicond.*, 2019, 40(8), 081502. http://doi.org/10.1088/1674-4926/40/8/081502

1. Introduction

The ferromagnetic semiconductor (Ga,Mn)As has been utilized to demonstrate proof-of-concept devices since its first synthesis in 1996[1]. (Ga,Mn)As exhibits hole mediated ferromagnetism, in which the localized Mn spin couples anti-ferromagnetically with valence band holes[2, 3]. In this review, we describe the recent research on (Ga,Mn)As, mainly focusing on the magnetization dynamics and its related phenomena. Comprehensive reviews of the synthesis, physics, and applications of ferromagnetic semiconductors have been updated continuously by many researchers, and are available elsewhere[4–6]. We present also recent results on the dynamics in a single crystalline ferromagnetic metal/semiconductor hybrid structures.

2. Properties of (Ga,Mn)As

Because the thermal-equilibrium solubility of Mn in GaAs is small, non-equilibrium growth method, i.e., low-temperature molecular-beam epitaxy at substrate temperature ~ 250 °C, is developed to synthesize single crystalline (Ga,Mn)As films with on the order of percent of nominal Mn composition *x*. Its p-type conductivity indicates that most of the Mn atoms (Mn_{Ga}) act as acceptors by replacing Ga atoms in divalent states (d^5 configuration with localized spin of 5/2)[7, 8]. A part of the Mn atoms, Mn_I, sit also at the interstitial sites due to the self-compensation effect[9]. The Mn_I acts as a double donor, and its spin couples antiferromagnetically with that of Mn_{Ga}[10]. The presence of Mn_I thus affects the electrical and magnetic properties[11]. The number of Mn_I can be reduced by post-growth annealing at ~ 200 °C through its diffusion towards surface[12].

The itinerant holes, which reside in the valence band of GaAs, mediate Ruderman-Kittel-Kasuya-Yosida (RKKY)-type exchange interaction among Mn spins[13], and bring about the ferromagnetism in (Ga,Mn)As[2, 3]. Therefore, there is a correlation between the electrical and magnetic properties, as explained by the *p-d* Zener model. The model is an adaption to the RKKY model specific to semiconducting materials, and can describe many properties of (Ga,Mn)As including the spin-orbit coupling related phenomena, such as the magneto-crystalline anisotropy, through band calculations based on effective mass approximations.

2.1. Curie temperature

In (Ga,Mn)As, the exchange interaction among As 4*p* and Mn 3*d* electrons (*p*–*d* exchange interaction) results in the ferromagnetic state. According to the *p*–*d* Zener model, the Curie temperature T_C is proportional to the effective Mn composition participating in the ferromagnetic order, and the density of state at the Fermi level. Therefore, T_C increases as the hole concentration *p* increases by decreasing the number of Mn_I through annealing. The enhancement of the annealing effect is expected for a (Ga,Mn)As nanowire because of its larger ratio of the surface region than films[14]. This was confirmed by magneto-transport measurements on a 310-nm wide nanowire of (Ga,Mn)As with x = 0.13, which exhibits a T_C of 200 K after annealing (as shown in Fig. 1)[15].

2.2. Magnetic anisotropy and anisotropic magnetoresistance effect

(Ga,Mn)As shows sizable magnetic anisotropy depending on the spontaneous magnetization *M*, *p*, and lattice strain. For example, a metallic (Ga,Mn)As film with compressive strain on a GaAs (001) substrate exhibits an in-plane easy axis for the magnetization, while that with tensile strain on an (In,Ga)As buffer layer shows perpendicular easy axis[16]. The in-plane magnetic anisotropy shows four-fold anisotropy along $\langle 100\rangle$ as well as two two-fold anisotropies along $[110]$ and $[\bar{1}10]$. Because (Ga,Mn)As exhibits a clear anomalous Hall effect and anisotrop-

Correspondence to: L Chen, lin.chen@ur.de
Received 10 JUNE 2019; Revised 30 JUNE 2019.
©2019 Chinese Institute of Electronics

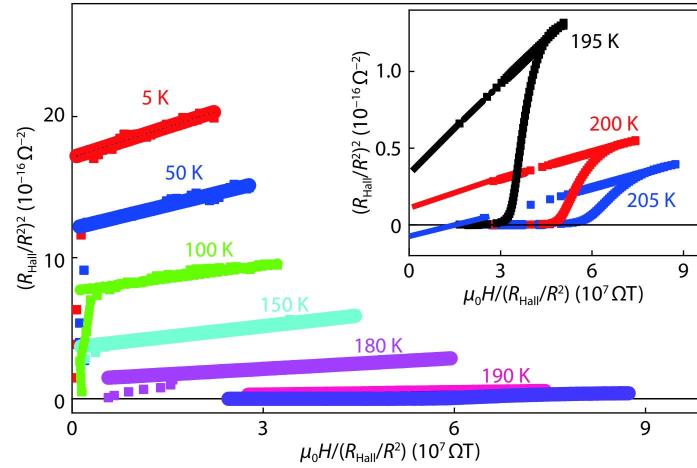

Fig. 1. (Colour online) Arrott plots at different temperatures for a 300 nm-wide Hall bar of (Ga,Mn)As. The inset shows a close-up view of the Arrott plots near the ferromagnetic transition, which confirms that T_C is slightly above 200 K. (Adapted from Ref. [15])

ic magnetoresistance (AMR)[1, 17–19], the direction and magnitude of the anisotropies can be determined by magneto-transport measurements[20]. Ferromagnetic resonance (FMR) can be also used to determine the magnetic anisotropies[21]. The origin of the anisotropies is explained by the spin-orbit interaction in the valence band of (Ga,Mn)As with (virtual) lattice strain[2, 3, 22–26].

2.3. Carrier localization

Magneto-transport measurements show that (Ga,Mn)As is in the vicinity of the metal-insulator transition (MIT)[27], and the interplay between magnetic properties and carrier localization has been probed experimentally. In doped semiconductors near MIT, there are two regions occupied by itinerant carriers and localized carriers[28]. In (Ga,Mn)As, the former region exhibits ferromagnetic behavior, and the latter superparamagnetic-like behavior[29]. The ratio between the two regions depends on the degree of the localization[30].

2.4. Electric-field effects

By making a capacitor structure with one of the two electrodes as a thin (Ga,Mn)As film, one can apply an electric-field onto (Ga,Mn)As to change p and the degree of MIT, which in turn alters the magnetic properties of (Ga,Mn)As due to carrier induced ferromagnetism. So far, the electric-field modulation of T_C[31], magnetic anisotropies[32], net magnetic moment[28], anomalous Hall coefficient[33], and Gilbert damping constant α has been demonstrated[30]. The electric-field effect is now being investigated also in ferromagnetic metals[34].

3. Ferromagnetic resonance (FMR) and related phenomena in (Ga,Mn)As-based structures

There is an excellent review on the magnetization precession in (Ga,Mn)As induced by optical means[6], and also a comprehensive review on FMR and spin-wave resonance in (Ga,Mn)As[35]. Here, we introduce recent topics of FMR and its related phenomena in (Ga,Mn)As-based structures.

FMR spectrum is usually measured as the derivative of the microwave absorption, which is well fitted by the derivative of the Lorentz function, $-(16I/\pi)\{\Delta H(H-H_R)/[4(H-H_R)^2+\Delta H^2]^2\}$, similar to other conventional ferromagnets. From the fitting, one can determine the absorption coefficient I, resonance field H_R, and the linewidth (the full width at half maximum) ΔH. The magnetization dynamics is known to be described by the Landau-Lifshitz-Gilbert (LLG) equation[36],

$$\frac{\mathrm{d}\boldsymbol{M}(t)}{\mathrm{d}t}=-\gamma\boldsymbol{M}(t)\times\mu_0\boldsymbol{H}_{\mathrm{eff}}+\frac{\alpha}{|\boldsymbol{M}|}\boldsymbol{M}(t)\times\frac{\mathrm{d}\boldsymbol{M}(t)}{\mathrm{d}t}, \tag{1}$$

and this is also the case for (Ga,Mn)As. Here, $\boldsymbol{M}$ is the spontaneous magnetization vector, t the time, μ_0 the magnetic constant, $\boldsymbol{H}_{\mathrm{eff}}$ the effective magnetic field, α the damping constant, γ the gyromagnetic ratio ($\gamma = g\mu_B/\hbar$), g the Landé g factor, μ_B the Bohr magneton, and $\hbar$ the Dirac constant. The first term on the right side of Eq. (1) corresponds to the magnetization precession about $\boldsymbol{H}_{\mathrm{eff}}$, while the second term to the relaxation of $\boldsymbol{M}$ towards $\boldsymbol{H}_{\mathrm{eff}}$. $\boldsymbol{H}_{\mathrm{eff}}$ is determined from the magnetostatic energy density F[35, 37],

$$\begin{aligned}F=&\frac{M}{2}\Big\{-2H[\cos\theta_M\cos\theta_H+\sin\theta_M\sin\theta_H\cos(\varphi_M-\varphi_H)]\\&+H_K\cos^2\theta_M-\frac{H_B}{2}\frac{3+\cos4\varphi_M}{4}\sin^4\theta_M\\&-H_U\sin^2\theta_M\sin^2\left(\varphi_M-\frac{\pi}{4}\right)-H_{U2}\sin^2\theta_M\sin^2\left(\varphi_M-\frac{\pi}{2}\right)\Big\}.\end{aligned} \tag{2}$$

as $\boldsymbol{H}_{\mathrm{eff}} = -\partial F/\partial \boldsymbol{M}$. Here $M = |\boldsymbol{M}|$, H the external magnetic field, H_K the effective perpendicular uniaxial magnetic anisotropy field including the demagnetizing field along [001], H_B the in-plane biaxial magnetic field along ⟨100⟩, H_U the in-plane uniaxial anisotropy along $[\bar{1}10]$, and H_{U2} the in-plane uniaxial anisotropy along [100]. The magnetic field angles θ_H and φ_H as well as the magnetization angles θ_M and φ_M are polar angles θ measured from the [001] and azimuthal angles φ measured from the [100] orientation. θ_M and φ_M are determined from the energy minimum conditions, $\partial F/\partial\theta_M = 0$, $\partial^2F/\partial\theta_M^2 > 0$, $\partial F/\partial\varphi_M = 0$, and $\partial^2F/\partial\varphi_M^2 > 0$. In a linear-response regime, the resonance condition is given by[38],

$$\left(\frac{\omega}{\gamma}\right)^2=\frac{1}{\mu_0M^2\sin^2\theta_M}\left[\frac{\partial^2F}{\partial\theta_M^2}-\left(\frac{\partial^2F}{\partial\theta_M\partial\varphi_M}\right)\right], \tag{3}$$

with $\omega = 2\pi f$. From the fitting of Eq. (3) to the magnetic-field angle dependence of H_R, one can determine the values of g and magnetic anisotropy fields.

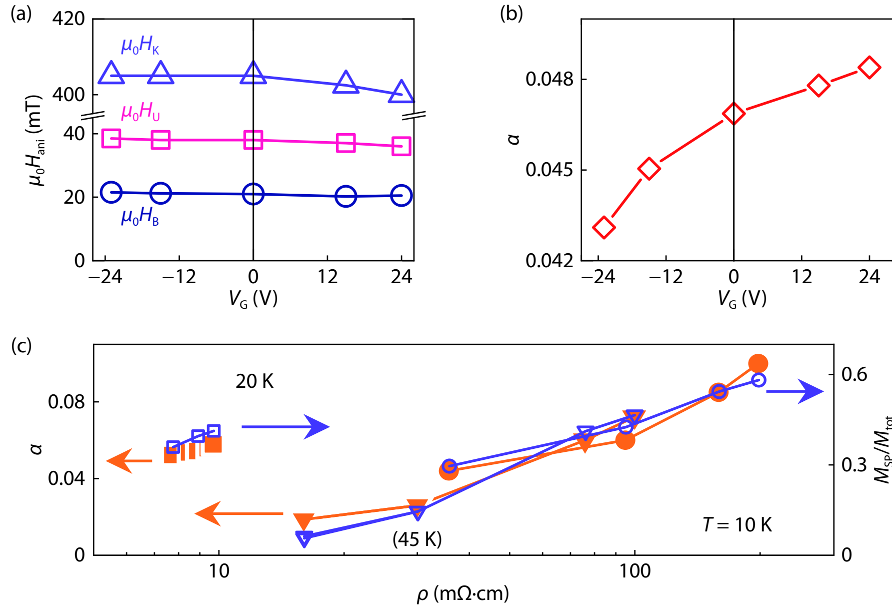

Fig. 2. (Colour online) Gate-voltage dependence of (a) magnetic anisotropy fields H_{ani} and (b) Gilbert damping constant α. (c) Damping constant α (closed symbols) and ratio of the superparamagnetic-like component M_{SP} to the total magnetic component M_{tot} (open symbols) as a function of resistivity ρ. Circles (triangles) are for the sample with $x = 0.075$ (0.068), whose ρ is changed by annealing. Squares are for the MIS structure, whose ρ is changed by applied gate voltage. (Adapted from Ref. [30])

The linewidth induced by intrinsic damping is expressed as[38],

$$\Delta H_{\text{G}} = \frac{\alpha}{M}\left(\frac{\partial^2 F}{\partial\theta_M^2} - \frac{1}{\sin^2\theta_M}\frac{\partial^2 F}{\partial\varphi_M^2}\right)\left|\frac{\text{d}(\omega/\gamma)}{\text{d}H_{\text{R}}}\right|^{-1}. \tag{4}$$

Extrinsic contributions such as the dispersion of the magnetic anisotropies and roughness as well as two-magnon scattering can also be included phenomenologically in the analysis of the magnetic-field angle θ_H (or φ_H) dependence of ΔH to determine the magnitude of α[39–42].

3.1. Electric-field effects on FMR spectra

The FMR measurements can be used to determine the magnitude of magnetic anisotropy fields, α, and g. By measuring the FMR spectra under electric-fields, one can determine the electric-field dependence of these parameters. The electric-field effects on the FMR spectra were investigated for a 4-nm thick (Ga,Mn)As film with $x = 0.13$ annealed at 200 °C for 10 min in a capacitor structure[30]. The maximum applied voltage V_G is 24 V, which corresponds to an electric field of ~4 MV/cm. The resistance changes by about ±10% by the application of ±24 V.

Figs. 2(a) and 2(b) show the V_G dependence of anisotropic fields H_{ani} and damping constant. The modulation of the magnetic anisotropy fields and g, whose values are expected to be determined by the spin-orbit interaction, is relatively small (~1%). On the other hand, α becomes larger by decreasing p through an electric field, and its modulation reaches ~12%, suggesting that the modulation is not determined only by the spin-orbit interaction. We measure the electrical resistance and magnetization under electric fields and those of some other samples with different conductivities in addition to α. As shown in Fig. 2(c), there is a clear correlation between the resistance, the portion of a superparamagnetic-like component, and α, i.e., a larger portion of the superparamagnetic-like component and larger α for samples with higher resistance. This observation suggests strongly that α in (Ga,Mn)As is determined mainly by the magnetic disorder induced by carrier localization.

The electric-field effect on α was also observed in a thin CoFeB/MgO structure[42], and the origin of the modulation is still to be elucidated.

3.2. Electrical detection of FMR

In conductive ferromagnets, the relationship between electric field $\boldsymbol{E}$ and current density $\boldsymbol{j}$ is phenomenologically expressed as[43],

$$\boldsymbol{E} = \rho\boldsymbol{j} + \left(\rho_{\parallel} - \rho_{\perp}\right)\boldsymbol{n}(\boldsymbol{j}\cdot\boldsymbol{n}) + \rho_{\text{H}}\boldsymbol{n}\times\boldsymbol{j}, \tag{5}$$

where ρ is the resistivity, $\boldsymbol{n}$ the unit magnetization vector ($\boldsymbol{n} = \boldsymbol{M}/M$), $\rho_\perp$ and $\rho_\parallel$ the resistivity perpendicular and parallel to $\boldsymbol{j}$, and ρ_{H} the anomalous Hall resistivity. The first term corresponds to Ohm's law, the second term to the AMR effect, and the third term to the anomalous Hall effect. The electric part of the microwave excites an oscillating current $\boldsymbol{j}$, and the magnetic part of the microwave causes the magnetization $\boldsymbol{n}$ to precess at the same frequency as $\boldsymbol{j}$. Thus, according to Eq. (5), a DC voltage is generated in the material under FMR.

We prepared a 20-nm thick (Ga,Mn)As film with $x = 0.065$ on a semi-insulating GaAs (001) substrate, and annealed it at 250 °C for 30 min. T_C of the (Ga,Mn)As was 118 K. We measured FMR spectra and DC voltages V along the [110] orientation simultaneously by sweeping H orthogonal to the [110] orientation at $f = 9$ GHz and at 45 K[37]. The electric-field component of the microwave was along the $[\bar{1}10]$ orientation and the magnetic-field component along the [110] orientation in our configuration. As shown in Fig. 3(b), the measured V is well fitted by the sum of the symmetric and anti-symmetric Lorentz functions, $L_{\text{sym}} = \Delta H^2/[4(H - H_{\text{R}})^2 + \Delta H^2]$ and $L_{\text{a-sym}} = -4\Delta H(H - H_{\text{R}})/[4(H - H_{\text{R}})^2 + \Delta H^2]$. The fitting gives identical H_{R} and ΔH with those determined from the FMR spectra shown in Fig. 3(a).

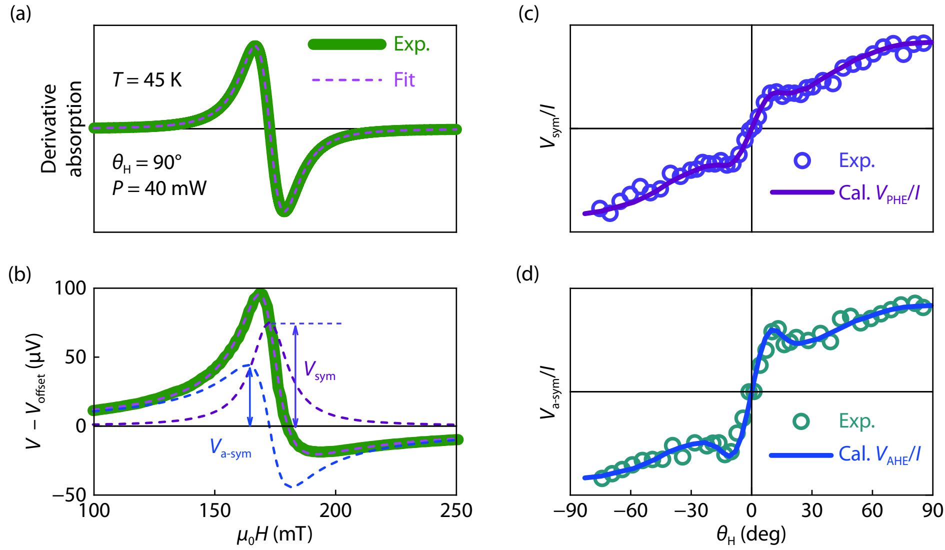

Fig. 3. (Colour online) (a) Ferromagnetic resonance and (b) DC voltage V spectrum obtained at temperature T = 45 K and magnetic field angle θ_H = 90° for (Ga,Mn)As/un-doped GaAs. Magnetic field angle θ_H dependence of (c) symmetric component V_{sym} and (d) anti-symmetric component $V_{a\text{-}sym}$ of the DC voltage, normalized by the microwave absorption coefficient I, which can be well fitted by the planar Hall effect and the anomalous Hall effect of (Ga,Mn)As. (Adapted from Ref. [37])

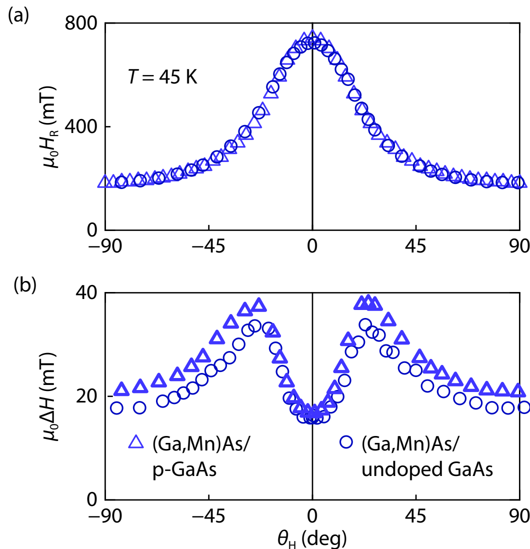

Fig. 4. (Colour online) The magnetic-field angle θ_H dependence of (a) the FMR resonant field H_R and (b) the linewidth ΔH for (Ga,Mn)As/p-GaAs and (Ga,Mn)As/undoped GaAs. The resonance fields for both samples are identical, while a larger linewidth is found for (Ga,Mn)As/p-GaAs, indicating the existence of spin pumping. (Adapted from Ref. [37])

According to Eq. (5), the transverse AMR effect (planar Hall effect) and the anomalous Hall effect contribute to V. The planar Hall effect reflects the real part of in-plane component of the dynamic magnetization Re(m_x), and thus exhibits a symmetric lineshape, V_{PHE} ~ Re(m_x). The anomalous Hall effect reflects the out-of-plane component Re(m_y), and thus exhibits an anti-symmetric lineshape, V_{AHE} ~ Re(m_y). As shown in Figs. 3(c) and 3(d), the magnetic-field angle dependence of V_{sym} and $V_{a\text{-}sym}$ can be well fitted by planar Hall effect and anomalous Hall effect of (Ga,Mn)As, respectively.

It was also shown that electrical detection of FMR is possible in (Ga,Mn)As through electric-field excitation[44].

3.3. Spin pumping and inverse spin Hall effect

Similar to metallic systems[45–47], the spin-pumping creates pure spin current from (Ga,Mn)As into adjacent p-GaAs. Due to the spin-orbit interaction in p-GaAs, the pure spin current is converted into a DC voltage through the inverse spin Hall effect, which is superimposed on the DC voltage induced by magnetogalvanic effects.

The measurements of the inverse spin Hall effect was done on virtually identical (Ga,Mn)As films as described in the previous section on a 20-nm thick p-GaAs layer with $p = 9.5 \times 10^{18}$ cm^{-3} grown on a semi-insulating GaAs substrate[37]. The measurement configuration and condition are the same as those in the previous section. We rotated the sample about the [110] orientation to measure the magnetic-field angle θ_H dependence of FMR and dc voltage. The presence of spin pumping is confirmed by the enhancement of ΔH of the (Ga,Mn)As/p-GaAs comparing to that of (Ga,Mn)As, which is shown in Fig. 4. The linewidth analysis gives the effective mixing conductance at the (Ga,Mn)As/p-GaAs to be 1.5×10^{19} cm^{-2}.

The DC voltage induced by inverse spin Hall effect V_{ISHE} is proportional to the damping term in Eq. (1), which can be derived as V_{ISHE} ~ Re(m_x)Im(m_y) – Im(m_x)Re(m_y). The lineshape of V_{ISHE} is symmetric, which is the same as the planar Hall effect. Note that, being different from V_{PHE}, V_{ISHE} results from the combination of the real and imaginary part of the dynamic magnetization. Thus, the separation of the signals induced by the two effects is possible by utilizing the different magnetic-field angle θ_H dependence of the two signals as shown in Fig. 5. The fitting reproduces well the experimental observation, and indicates contributions of 12% from the inverse spin Hall effect and 88% from the planar Hall effect to symmetric DC voltage[37]. This separation method has been applied to other material systems[48–50].

4. Spin-orbit torques in single crystalline Fe/GaAs (001) hybrid structures

Due to the crystal and structural symmetry breaking in a

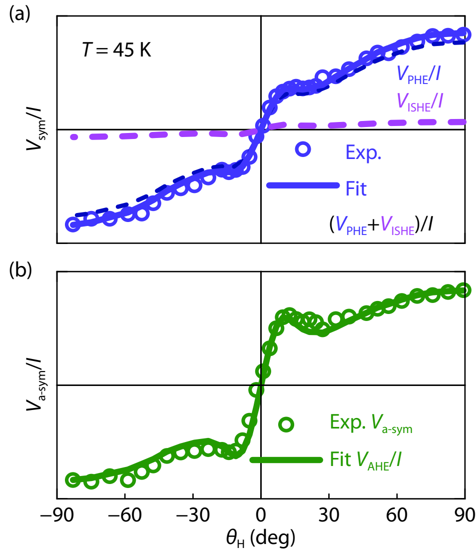

Fig. 5. (Colour online) Angular dependence of the DC voltage for (Ga,Mn)As/p-GaAs.Magnetic field angle θ_H dependence of (a) symmetric component V_{sym} and (b) anti-symmetric component $V_{a\text{-}sym}$ of the DC voltage, normalized by the microwave absorption coefficient *I*. Dotted and dashed lines in (a) show the θ_H dependence of the DC voltages induced by the inverse spin Hall effect V_{ISHE}/I and planar Hall effect V_{PHE}/I, where the ratio of the magnitudes of V_{ISHE} and V_{PHE} is adjusted to reproduce the experimental result. Solid line represents total contributions, $V_{ISHE}/I + V_{PHE}/I$. Solid line in (b) shows the θ_H dependence of the DC voltage induced by the anomalous Hall effect V_{AHE} normalized by *I*. (Adapted from Ref. [37])

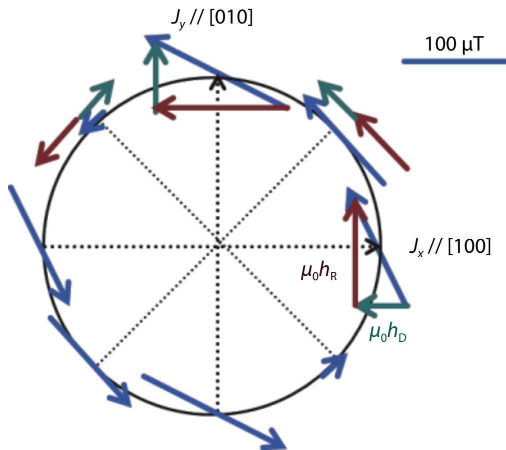

Fig. 6. (Colour online) Experimentally determined magnitude and direction of the in-plane spin-orbit fields, which are normalized by a unit current density of 10^{11} A/m^2.

strained (Ga,Mn)As film, one can induce the effective spin-orbit magnetic field in (Ga,Mn)As by applying electric current, which was utilized to manipulate the magnetization direction and to excite FMR[44, 51, 52]. Thus, one can imagine not making GaAs ferromagnetic, but putting a layer of single crystalline ferromagnetic metal on top of GaAs[53, 54]. Here, we focus on the FMR induced by spin-orbit torques in a Fe film on GaAs (001) at room temperature. A thin single crystalline Fe film can be grown on GaAs by MBE thanks to relatively small lattice mismatch (~ 1.4%) between the two materials[53, 54]. Fe/GaAs heterostructure has long been used for spin-injection experiments[55–57], and interest in the system has recently been revived in view of spin-orbitronics due to the presence of Bychkov-Rashba- and Dresselhaus-like spin-orbit interactions at the interface[58]. The effective in-plane spin-orbit fields, $\boldsymbol{h}_{eff}$, in momentum space can be written as[59],

$$\mu_0 \boldsymbol{h}_{\rm eff} = \frac{1}{\mu_{\rm B}}\left(-\beta k_x - \alpha k_y, \alpha k_x + \beta k_y\right), \tag{6}$$

where k_x (k_y) is a [100] ([010]) component of the wavevector $\boldsymbol{k}$, and α (β) characterizes the strength of the Bychkov-Rashba (Dresselhaus) spin-orbit interaction. The presence of the interfacial spin-orbit interaction was evidenced previously by tunneling anisotropic magnetoresistance measurements in a Au/GaAs/Fe trilayer structure[53].

4.1. Quantifying the interfacial spin-orbit field at the Fe/GaAs interface

The strength of the interfacial spin-orbit fields at the Fe/GaAs interface can be quantified using spin-orbit-torque FMR (SO-FMR). The applied RF current to Fe/GaAs produces RF spin-orbit fields, which induce magnetization precession when the resonance condition is fulfilled. The precession results in the periodic change in resistance with precessional frequency through the magnetogalvanic effect in Fe, and thus produces DC voltage *V* (Eq. (5))[44].

The sample used for SO-FMR measurements is a 5-nm thick single crystalline Fe grown by MBE on undoped GaAs (001). The Fe layer was patterned into stripes (6.4 × 100 μm^2) along different crystal orientations of GaAs, i,e., [100], [010], [110], and $[\bar{1}10]$ orientations. The DC voltage *V* was measured at RF current with frequency of 12 GHz as functions of current density up to ~1.9×10^{11} A/m^2 and the direction φ_H of an external in-plane magnetic field by sweeping the external field. The external magnetic-field dependence of *V* contains both symmetric and anti-symmetric lineshapes, which can be decomposed into the symmetric and anti-symmetric Lorentz functions. The symmetric component results mainly from the out-of-plane components of effective spin-orbit fields and the anti-symmetric component from the in-plane components. By analyzing the magnetization-angle φ_M dependence of the anti-symmetric component of *V*, one can determine the crystal-orientation dependence of the magnitude of the effective spin-orbit fields as shown in Fig. 6 at $j = 10^{11}$ A/m^2[58]. The obtained results are explained by the coexistence of Bychkov-Rashba ($\boldsymbol{h}_R$) and Dresselhaus ($\boldsymbol{h}_D$) components of spin-orbit fields in agreement with theoretical predictions.

The spin galvanic effect induced by spin pumping at Fe/GaAs spin-orbit interface was also demonstrated by exciting FMR using an out-of-plane component of an Oersted field in a coplanar waveguide (putting Fe wires a gap between the signal and ground lines of a coplanar waveguide)[58]. Similar observations have been reported for Bi/Ag and $LaAlO_3/SrTiO_3$ Rashba interface[60, 61].

4.2. Electric-field control of interfacial spin-orbit fields

The magnitude of β and α at the Fe/GaAs interface depends linearly on the interfacial electric-field. Thus, it is possible to control the effective spin-orbit field by an external electric-field[62]. The sample investigated in this study was an Fe (4 nm)/n-GaAs (electron concentration, $n = 4 \times 10^{16}$ cm^{-3}) Schottky junction. The DC voltage *V* induced by SOT-FMR was measured under a gate voltage V_G applied through the depleted n-GaAs underneath Fe, and the strength of spin-orbit effective

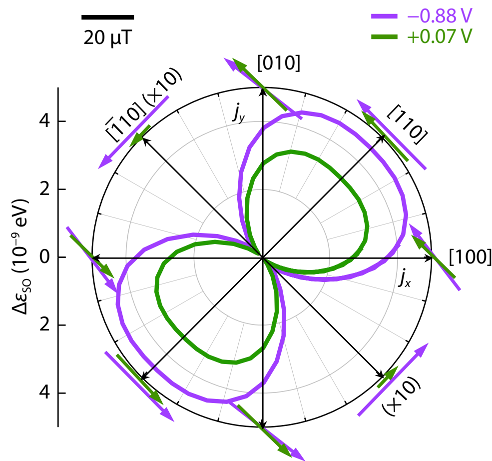

Fig. 7. (Colour online) Polar plot of in-plane spin-orbit fields under different gate-voltages. The arrows represent direction and relative strength of $\boldsymbol{h}_{\rm eff}$, and the solid lines represent the spin-orbit energy splitting. (Adapted from Ref. [62])

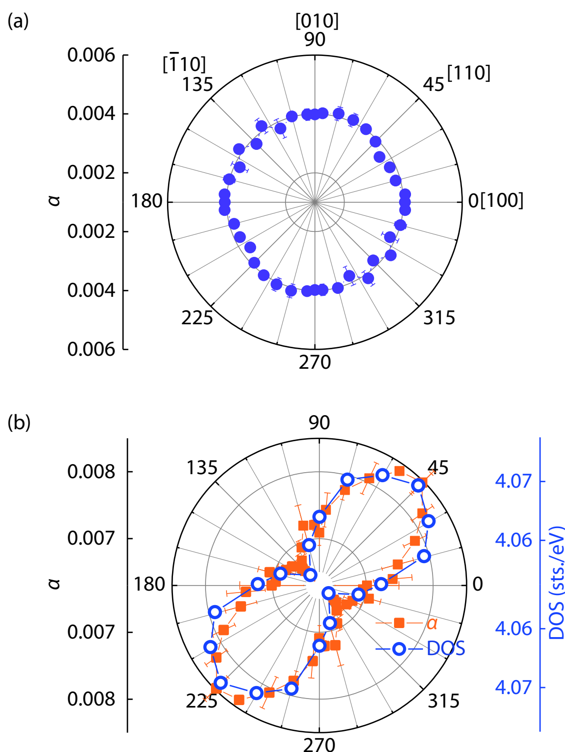

Fig. 8. (Colour online) Magnetic-field angle φ_H dependence of the damping constant α for Fe thickness of (a) 1.9 nm and (b) 1.3 nm. Isotropic damping is observed for 1.9 nm-Fe. However, for Fe thickness of 1.3 nm, a larger α along <110> is observed, and α gradually decreases until approaching $\langle\bar{1}10\rangle$. The anisotropic damping shows 2-fold symmetry, which results from the anisotropic density of states at the Fe/GaAs interface, as shown by open symbols in (b). (Adapted from Ref. [66])

field was determined by the method described above. Fig. 7 shows the polar plot of the effective spin-orbit fields at $V_{\rm G}$ = −0.88 V and +0.07 V (arrows are field vectors and lines are spin-orbit energy splitting $\Delta\varepsilon_{\rm SO} = 2\mu_{\rm B}\mu_0|\boldsymbol{h}_{\rm eff}|$). It clearly exhibits the electric-field modulation of the spin-orbit field vectors. For [100] and [010] orientations, both the direction and strength of the fields is modified $V_{\rm G}$, while for [110] and [$\bar{1}$10] orientations, only the strength of the fields is modified. The result shows also that the modulation of the Bychkov-Rashba spin-orbit fields is several-time larger than that of the Dresselhaus spin-orbit field.

The electric-field modulation of the interfacial spin-orbit effects is attracting much attention also from the view point of practical applications. For instance, the electric-field induced precessional magnetization switching through the modulation of the interfacial magnetic anisotropy was demonstrated, and this switching scheme is fast with low-power consumption[63].

4.3. Emergence of anisotropic Gilbert damping at Fe/GaAs interface

The interplay of Bychkov-Rashba and Dresselhaus spin-orbit interaction can modify the density of states at the Fe/GaAs interface. This has caused a rich variety of interfacial spin-orbit related phenomena. It has been found that the symmetry of the anisotropic magneto-resistance[64], the polar magneto-optic Kerr effect[65] and the Gilbert damping[66] is governed by the two-fold interfacial C_{2v} symmetry rather than its bulk fold C_{4v} symmetry when the thickness of Fe is decreased to a few monolayers. Here we show the emergence of anisotropic damping in ultrathin Fe film on GaAs (001).

Fig. 8(a) shows the angular dependence of Gilbert damping for Fe thickness of 1.9 nm determined by analyzing the in-plane magnetic angle $\varphi_{\rm H}$ dependence and the microwave frequency f dependence of the linewidth. Isotropic behavior is observed for 1.9 nm Fe on GaAs. However, clear anisotropic Gilbert damping has been found when the Fe thickness is reduced to 1.3 nm as shown in Fig. 8(b). The anisotropic damping shows two-fold symmetry, coinciding with the symmetry observed for tunneling anisotropic magnetoresistance[53], crystalline anisotropic magnetoresistance[64] and the polar magneto-optic Kerr effect[65], can be explained in terms of the anisotropic density of states (open symbols in Fig. 8(b)) induced by the interfacial spin-orbit interaction.

5. Conclusion

We have described the fundamental properties of (Ga,Mn)As focusing on its ferromagnetic-resonance (FMR) related phenomena such as the spin pumping and the electric-field modulation of the damping constant. We have described also recent topics on FMR-related phenomena in single crystalline Fe/GaAs structures such as the electric-field modulation of the interfacial spin-orbit fields and the emergence of the anisotropic damping in the structures with an ultrathin Fe. In both systems, (Ga,Mn)As and Fe/GaAs, the observation of the magnetization dynamics provides us the opportunities to investigate a variety of physics based on their spin-orbit interaction.

Acknowledgements

The authors thank T. Dietl, J. Fabian, M. Gmitra, S. Mankovsky, H. Ebert, M. Kronseder, D. Schuh, D. Bougeard for fruitful discussions. L. C. thanks the German Science Foundation (DFG) via SFB 1277 for support. The work at Tohoku University was partially supported by Grant-in-Aids from MEXT and JSPS.

References

[1] Ohno H, Shen A, Matsukura F, et al. (Ga,Mn)As: A new diluted

magnetic semiconductor based on GaAs. Appl Phys Lett, 1996, 69, 363
[2] Dietl T, Ohno H, Matsukura F, et al. Zener model description in ferromagnetism in zinc-blende magnetic semiconductors. Sience, 2000, 287, 1019
[3] Diet T, Ohno H, Matsukura F. Hole-mediated ferromagnetism in tetrahedrally coordinated semiconductors. Phys Rev B, 2001, 63, 195205
[4] Matsukura F, Ohno H. Chapter 19 Molecular beam epitaxy of III–V semiconductors in molecular beam epitaxy from research to mass production (Henini M, Ed.). Amsterdam: Elsevier, 2013
[5] Dietl T, Ohno H. Dilute ferromagnetic semiconductors: Physics and spintronic structures. Rev Mod Phys, 2014, 86, 187
[6] Jungwirth T, Wunderlich J, Novák, V, et al. Spin-dependent phenomena and device concepts explored in (Ga,Mn)As. Rev Mod Phys, 2014, 86, 855
[7] Schneider J, Kaufmann, Y, Wilkening W, et al. Electronic structure of neutral manganese acceptor in gallium arsenide. Phys Rev Lett, 1987, 59, 240
[8] Szczytko J, Teardowski J, Świątek K, et al. Mn impurity in $Ga_{1-x}Mn_xAs$ epilayers. Phys Rev B, 1999, 60, 8304
[9] Yu K M, Walukiewicz W, Wojtowicz T, et al. Effect of the location of Mn sites in ferromagnetic $Ga_{1-x}Mn_xAs$ on its Curie temperature. Phys Rev B, 2002, 65, 201303
[10] Blinowski J, Kacman P. Spin interactions of interstitial Mn ions in ferromagnetic GaMnAs. Phys Rev B, 2003, 67, 121204(R)
[11] Wojtowicz T, Furdyna J K, Liu X, et al. Electronic effects determining the formation of ferromagnetic $III_{1-x}Mn_xV$ alloys during epitaxial growth. Physica E, 2004, 25, 171
[12] Edmonds K W, Bogusławski P, Wang K Y, et al. Mn interstitial diffusion in (Ga,Mn)As. Phys Rev Lett, 2004, 92, 037201
[13] Souma S, Chen L, Oszwałdowski R. Fermi level position, Coulomb gap, and Dresselhaus splitting in (Ga,Mn)As. Sci Rep, 2016, 6, 27266
[14] Fid K F, Sheu B L, Maksimov O, et al. Nanoengineered Curie temperature in laterally patterned ferromagnetic semiconductor heterostructures. Appl Phys Lett, 2005, 86, 152505
[15] Chen L, Yan X, Yang F, et al. Enhancing the Curie temperature of ferromagnetic semiconductor (Ga,Mn)As to 200 K via nanostructure engineering. Nano Lett, 2011, 11, 2584
[16] Shen A, Ohno H, Matsukura F, et al. Epitaxy of (Ga,Mn)As, a new diluted magnetic semiconductor based on GaAs. J Cryst Growth, 1997, 175/176, 1069
[17] Jungwirth T, Niu Q, MacDonald A H. Anomalous Hall effect in ferromagnetic semiconductors. Phys Rev Lett, 2002, 88, 207208
[18] Baxter D V, Ruzmetov D, Scherschligt J, et al. Anisotropic magnetoresistance in $Ga_{1-x}Mn_xAs$. Phys Rev B, 2002, 65, 212407
[19] Tang H X, Kawakami R K, Awschalom D D, et al. Giant planar Hall effect in epitaxial (Ga,Mn)As devices. Phys Rev Lett, 2003, 90, 107201
[20] Pappert K, Hümpfner S, Wenisch J, et al. Transport characterization of the magnetic anisotropy of (Ga,Mn)As. Appl Phys Lett, 2007, 90, 062109
[21] Yamada T, Chiba D, Matsukura F, et al. Magnetic anisotropy in (Ga,Mn)As probed by magnetotransport measurements. Phys Status Solidi C, 2006, 3, 4086
[22] Abolfath M, Jungwirth T, Brum J, et al. Theory of magnetic anisotropy in $III_{1-x}Mn_xV$ ferromagets. J Magn Magn Mater, 2008, 320, 1190
[23] Birowska M, Śliwa C, Majewski J A, et al. Origin of bulk uniaxial anisotropy in zinc-blende dilute magnetic semiconductors. Phys Rev Lett, 2012, 108, 237203
[24] Zemen J, Kučera J, Olejník K, et al. Magnetocrystalline anisotropies in (Ga,Mn)As: Systematic theoretical study and comparison with experiment. Phys Rev B, 2009, 80, 155203
[25] Stefanowicz W, Śliwa C, Alekshkevych P, et al. Magnetic anisotropy of epitaxial (Ga,Mn)As on (113)A GaAs. Phys Rev B, 2010, 81, 155203
[26] Sawicki M, Poselkov O, Sliwa C, et al. Cubic anisotropy in (Ga,Mn)As layers: Experiment and theory. Phys Rev B, 2018, 97, 184403
[27] Oiwa A, Katsumoto S, Endo A, et al. Nonmetal-metal-nonmetal transition and large negative magnetoresistance in (Ga,Mn)As/GaAs. Solid State Commun, 1997, 103, 209
[28] Dietl T. Interplay between carrier localization and magnetism in diluted magnetic and ferromagnetic semiconductors. J Phys Soc Jpn, 2008, 77, 031005
[29] Sawicki M, Chiba D, Korbecka A. Experimental probing of the interplay between ferromagnetism and localization in (Ga,Mn)As. Nat Phys, 2009, 6, 22
[30] Chen L, Matsukura F, Ohno, H. Electric-field modulation of damping constant in a ferromagnetic semiconductor (Ga,Mn)As. Phys Rev Lett, 2015, 115, 057204
[31] Chiba D, Matsukura F, Ohno H. Electric-field control of ferromagnetism in (Ga,Mn)As. Appl Phys Lett, 2006, 89, 162505
[32] Chiba D, Sawicki M, Nishitani Y, et al. Magnetization vector manipulation by electric fields. Nature, 2008, 455, 515
[33] Chiba D, Werpachowska, A, Endo M, et al. Anomalous Hall effect in field-effect structures of (Ga,Mn)As. Phys Rev Lett, 2010, 104, 106601
[34] Matsukura F, Tokura Y, Ohno H. Control of magnetism by electric fields. Nat Nanotechnol, 2015, 10, 209
[35] Liu X, Furdyna J K. Ferromagnetic resonance in $Ga_{1-x}Mn_xAs$ dilute magnetic semiconductors. J Phys: Condens Matter, 2006, 18, R245
[36] Gilbert T L. A phenomenological theory of damping in ferromagnetic materials. IEEE Trans Magn, 2004, 40, 3443
[37] Chen L, Matsukura F, Ohno H. Direct-current voltages in (Ga,Mn)As structures induced by ferromagnetic resonance. Nat Commun, 2013, 4, 2055
[38] Suhl H. Ferromagnetic resonance in nickel ferrite between one and two kilomegacycles. Phys Rev, 1955, 97, 555
[39] Mizukami S, Ando Y, Miyazaki, T. The study on ferromagnetic resonance linewidth for NM/80NiFe/NM (NM = Cu, Ta, Pd and Pt) films. Jpn J Appl Phys, 2001, 40, 580
[40] Arias R, Mills D L. Extrinsic contributions to the ferromagnetic resonance response of ultrathin films. Phys Rev B, 1999, 60, 7395
[41] Lindner J, Barsukov, I, Raeder C, et al. Two-magnon damping in thin films in case of canted magnetization: Theory versus experiment. Phys Rev B, 2009, 80, 224421
[42] Okada A, Kanai S, Yamanouchi M, et al. Electric-field effects on magnetic anisotropy and damping constant in Ta/CoFeB/MgO investigated by ferromagnetic resonance. Appl Phys Lett, 2014, 105, 052415
[43] Juretschke H J. Electromagnetic theory of dc effects in ferromagnetic resonance. J Appl Phys, 1960, 31, 1401
[44] Fang D, Kurebayashi H, Wunderlich J, et al. Spin-orbit-driven ferromagnetic resonance. Nat Nanotechnol, 2011, 6, 413
[45] Mizukami S, Ando Y, Miyazaki T. Effect of spin diffusion on Gilbert damping for a very thin permalloy layer in Cu/permalloy/Cu/Pt films. Phys Rev B, 2002, 66, 104413
[46] Tserkovnyak Y, Brataas A, Bauer G E W. Enhanced Gilbert damping in thin ferromagnetic films. Phys Rev Lett, 2002, 88, 117601
[47] Saitoh E, Ueda M, Miyajima, H, et al. Conversion of spin current into charge current at room temperature: Inverse spin-Hall effect. Appl Phys Lett, 2006, 88, 182509
[48] Chen L, Ikeda S, Matsukura F, et al. DC voltages in Py and Py/Pt under ferromagnetic resonance. Appl Phys Express, 2014, 7, 013002
[49] Nakayama H, Chen L, Chang H W, et al. Inverse spin Hall effect in Pt/(Ga,Mn)As. Appl Phys Lett, 2015, 106, 222405
[50] Isogami S, Tsunoda M. Enhanced inverse spin-Hall voltage in

(001) oriented Fe_4N/Pt polycrystalline films without contribution of planar-Hall effect. Jpn J Appl Phys, 2016, 55, 043001
[51] Chernyshov A, Overby M, Liu X, et al. Evidence for reversible control of magnetization in a ferromagnetic material by means of spin-orbit magnetic field. Nat Phys, 2009, 5, 656
[52] Endo M, Matsukura F, Ohno H. Current induced effective magnetic field and magnetization reversal in uniaxial anisotropy (Ga,Mn)As. Appl Phys Lett, 2010, 97, 222501
[53] Moser J, Matos-Abiague A, Schuh D, et al. Tunneling anisotropic magnetoresistance and spin-orbit coupling in Fe/GaAs/Au tunnel junctions. Phys Rev Lett, 2007, 99, 056601
[54] Gmitra M, Matos-Abiague A, Draxl C, et al. Magnetic control of spin-orbit fields: A first-principles study of Fe/GaAs junctions. Phys Rev Lett, 2013, 111, 036603
[55] Žutić I, Fabian J, Das Sarma S. Spintronics: Fundamentals and applications. Rev Mod Phys, 2004, 76, 323
[56] Zhu H J, Ramsteiner M, Kostial H, et al. Room-temperature spin injection from Fe into GaAs. Phys Rev Lett, 2001, 87, 016601
[57] Lou X, Adelmann C, Crooker S A, et al. Electrical detection of spin transport in lateral ferromagnet-semiconductor devices. Nat Phys, 2007, 3, 197
[58] Chen L, Decker M, Kronseder M, et al. Robust spin-orbit torque and spin-galvanic effect at the Fe/GaAs(001) interface at room temperature. Nat Commun, 2016, 7, 13802
[59] Fabian J, Matos-Abiague A, Ertler C, et al. Semiconductor spintronics. Acta Physics Slovaca, 2007, 57, 565
[60] Sánchez J C R, Vila L, Desfonds G, et al. Spin-to-charge conversion using Rashba coupling at the interface between non-magnetic materials. Nat Commun, 2013, 4, 2944
[61] Lesne E, Fu Y, Oyarzun S, et al. Highly efficient and tunable spin-to-charge conversion through Rashba coupling at oxide interfaces. Nat Mater, 2016, 15, 1261
[62] Chen L, Gmitra M, Vogel M, et al. Electric-field control of interfacial spin-orbit fields. Nat Elect, 2018, 1, 350
[63] Liu H, Lim W L, Urazhdin. Control of current-induced spin-orbit effects in a ferromagnetic heterostructure by electric field. Phys Rev B, 2014, 89, 220409(R)
[64] Hupfauer T, Matos-Abiague A, Gmitra M, et al. Emergence of spin-orbit fields in magnetotransport of quasi-two-dimensional iron on gallium arsenide. Nat Commun, 2015, 6, 7374
[65] Buchner M, Högl P, Putz S, et al. Anisotropic polar magneto-optic Kerr effect of ultrathin Fe/GaAs (001) layers due to interfacial spin-orbit interaction. Phys Rev Lett, 2016, 117, 157202
[66] Chen L, Mankovsky S, Wimmer S, et al. Emergence of anisotropic Gilbert damping in ultrathin Fe layers on GaAs(001). Nat Phys, 2018, 14, 490